





PAPER

Electronic structure of stoichiometric and oxygen-deficient ferroelectric
 $\text{Hf}_{0.5}\text{Zr}_{0.5}\text{O}_2$

To cite this article: T V Perevalov *et al* 2018 *Nanotechnology* **29** 194001

View the [article online](#) for updates and enhancements.

Electronic structure of stoichiometric and oxygen-deficient ferroelectric $\text{Hf}_{0.5}\text{Zr}_{0.5}\text{O}_2$

T V Perevalov^{1,2} , D R Islamov^{1,2} , V A Gritsenko^{1,2,3}  and I P Prosvirin⁴ 

¹Rzhanov Institute of Semiconductor Physics SB RAS, 630090 Novosibirsk, Russia

²Novosibirsk State University, 630090 Novosibirsk, Russia

³Novosibirsk State Technical University, 630073, Novosibirsk, Russia

⁴Boreskov Institute of Catalysis SB RAS, 630090, Novosibirsk, Russia

E-mail: timson@isp.nsc.ru

Received 29 November 2017, revised 28 December 2017

Accepted for publication 2 February 2018

Published 13 March 2018



CrossMark

Abstract

The electronic structure of oxygen-deficient $\text{Hf}_{0.5}\text{Zr}_{0.5}\text{O}_2$ in the non-centrosymmetric orthorhombic (ferroelectric) phase was investigated by means of x-ray photoelectron spectroscopy and first-principle density functional theory calculations. It was established that a peak in the photoelectron spectra observed at an energy above the valence band top of ferroelectric $\text{Hf}_{0.5}\text{Zr}_{0.5}\text{O}_2$ in ion-etched samples was due to oxygen vacancies. A method for evaluating the oxygen vacancies concentration in the material from the comparison of experimental and theoretical photoelectron spectra of the valence band is proposed. It is found that oxygen polyvacancies are not formed in ferroelectric $\text{Hf}_{0.5}\text{Zr}_{0.5}\text{O}_2$: an energy-favorable spatial arrangement of several oxygen vacancies in the crystal corresponds to the configuration formed by noninteracting vacancies distant from each other. The oxygen vacancies in five charged states were simulated. The electron levels in the bandgap caused by charged oxygen vacancies indicate that any type of oxygen vacancies in ferroelectric $\text{Hf}_{0.5}\text{Zr}_{0.5}\text{O}_2$ can capture both electrons and holes, i.e. can act as an amphoteric localization center for charge carriers.

Keywords: electronic structure, oxygen vacancy, ferroelectrics, XPS, charge localization, *ab initio* calculations

(Some figures may appear in colour only in the online journal)

1. Introduction

Presently, the solid dielectric solution of hafnium and zirconium oxides ($\text{Hf}_{0.5}\text{Zr}_{0.5}\text{O}_2$) is of great interest among material science experts in silicon microelectronics. That interest is mainly due to the discovery of a ferroelectric effect in thin (~ 10 nm) $\text{Hf}_{0.5}\text{Zr}_{0.5}\text{O}_2$ films, finding of which makes such films potentially interesting for the use as an active medium of nonvolatile ferroelectric random access memory (FRAM) devices [1]. The ferroelectric properties of $\text{Hf}_{0.5}\text{Zr}_{0.5}\text{O}_2$ are believed to be due to the noncentrosymmetric orthorhombic phase stabilization, ($\text{Pbc}2_1$) ($\text{o-Hf}_{0.5}\text{Zr}_{0.5}\text{O}_2$), metastable under standard conditions. The discovery of ferroelectric properties of thin submicrometer-scaled films of the HfO_2 -based material, already being used in the silicon technology, opens up a possibility of replacing perovskite film

structures in FRAM [1]. Despite the extensive studies of the ferroelectric-response phenomenon in $\text{o-Hf}_{0.5}\text{Zr}_{0.5}\text{O}_2$, the issues concerning the impact of defects in the electronic structure of $\text{o-Hf}_{0.5}\text{Zr}_{0.5}\text{O}_2$, as well as ferroelectric phase stabilization and degradation of this material, remain a poorly studied matter.

It is a known fact that the electronic properties of high- κ oxide dielectrics are substantially determined by intrinsic defects, namely by oxygen vacancies [2, 3]. The oxygen loss commonly generates the defect states in the oxide bandgap with a drastic conductivity variation [4–6]. It was proved that the oxygen vacancies in ZrO_2 and HfO_2 act as traps for charge carriers [7, 8]. The traps play different roles in high- κ oxide-based devices. When the high- κ is used as gate dielectric, traps increase conductance. Localization of electrons or holes on traps shifts the threshold voltage, and leads to MOSFET

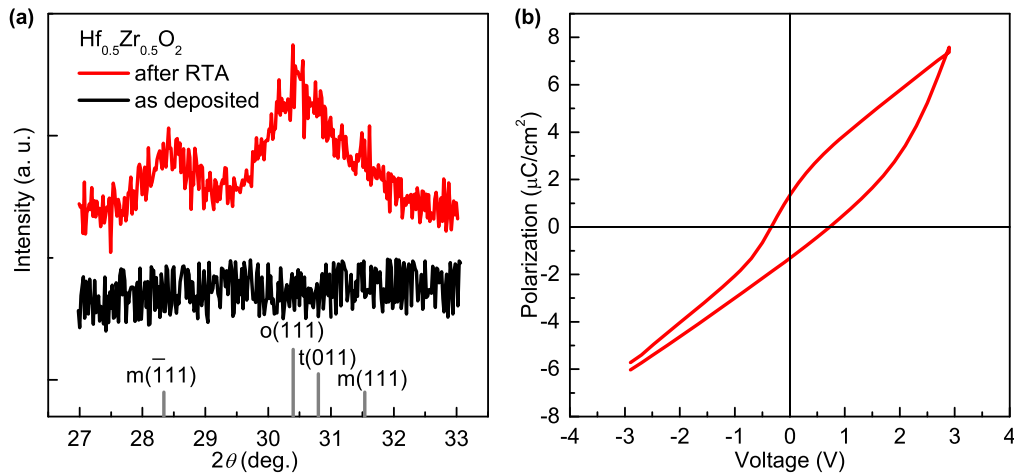


Figure 1. (a) XRD spectra of as deposited and after RTA $\text{Hf}_{0.5}\text{Zr}_{0.5}\text{O}_2$ films. [10] (2015) (© Pleiades Publishing, Inc. 2015). With permission of Springer. (b) Polarization-voltage loops for Pt/f- $\text{Hf}_{0.5}\text{Zr}_{0.5}\text{O}_2$ /TiN structures measured at room temperature. Reproduced with permission from [14]. Reproduced from [15]. © IOP Publishing Ltd. CC BY 3.0.

degradation. On the other hand, in active layers of resistive random access memory traps act as precursors of the conductive filament during switch from high-resistance state to low-resistance state. In this case, the traps are used for device switching and information storing. So, it is very important to know atomic and electronic structure of defects in high- κ dielectrics to meet requirements of electronic devices during synthesis processes.

Since ZrO_2 and HfO_2 have similar electronic structures, it should be expected that the electronic properties of their solid solution are also determined by the oxygen vacancies. This expectation argument is feasible to solve using the first-principle quantum-chemical modeling, but the electronic structure of oxygen vacancies in ferroelectric f- $\text{Hf}_{0.5}\text{Zr}_{0.5}\text{O}_2$ has not been studied yet this way.

The current-voltage characteristics simulation of f- $\text{Hf}_{0.5}\text{Zr}_{0.5}\text{O}_2$ thin film allows making a reasoned assumption that the traps responsible for charge transport are caused by oxygen vacancies [9, 10]. It was found that an increase of oxygen vacancies concentration in the ferroelectric HfO_2 films doped with strontium results in an increase of leakage currents in the functional structures based on this material, and it also adversely affects its ferroelectric properties [11]. Thus, understanding the electronic structure of the oxygen vacancies in f- $\text{Hf}_{0.5}\text{Zr}_{0.5}\text{O}_2$ can provide valuable information, particularly, useful for the optimization of f- $\text{Hf}_{0.5}\text{Zr}_{0.5}\text{O}_2$ synthesis processes aimed at FRAM elements formation of.

Today, the quantum-chemical calculations made within the density functional theory (DFT) offer a reliable tool for studying electronic the structure of defects in solids. The problem of bandgap underestimation is solved by using nonlocal exchange-correlation functionals, for example, involving the contribution due to the exact Hartree-Fock exchange (the so-called hybrid functionals). One of the experimental techniques for studying the electronic structure of defects in solids is photoelectron spectroscopy. One can use the phenomenon of metal cations partial reduction in Ar^+ -etched samples, as it was observed in ZrO_2 [12] and

HfO_2 [13] films, as a method of oxygen vacancies generation in oxide structure.

The purpose of the present study is investigating the oxygen vacancies electronic structure in the non-centrosymmetric orthorhombic phase of $\text{Hf}_{0.5}\text{Zr}_{0.5}\text{O}_2$ by means of x-ray photoelectron spectroscopy (XPS) and the first-principle calculations using the hybrid DFT.

2. Materials and methods

The 10 nm thickness f- $\text{Hf}_{0.5}\text{Zr}_{0.5}\text{O}_2$ film was synthesized on (100) Si substrates using the atomic layer deposition process at the temperature of 240 °C with the use of $\text{Hf}[\text{N}(\text{CH}_3)(\text{C}_2\text{H}_5)]_4$ (TEMAH) and $\text{Zr}[\text{N}(\text{CH}_3)(\text{C}_2\text{H}_5)]_4$ (TEMAZ) precursors and oxidizer H_2O as described in [10, 14, 15].

The film thickness and stoichiometry were controlled by laser ellipsometry and Rutherford backscattering spectroscopy methods. The synthesized film was subjected to the rapid thermal annealing (RTA) at 400 °C for 30 s in the N_2 atmosphere. The crystalline structures of as deposited and annealed films were examined by symmetrical x-ray diffraction (XRD) using ARL X'TRA tool (Thermo Scientific) utilizing $\text{CuK}\alpha$ radiation. The XRD pattern of the annealed $\text{Hf}_{0.5}\text{Zr}_{0.5}\text{O}_2$ film shows its polycrystalline structure (figure 1(a)). The most intense XRD peak is formed by the presence of overlapping reflections associated with the tetragonal (P42/nmc) and the non-centrosymmetric orthorhombic phase (Pbc21). Polarization-voltage loops, obtained by integration of displacement current response in reply to the stepped triangle voltage and depicted in figure 1(b), prove the presence of ferroelectric phase in annealed $\text{Hf}_{0.5}\text{Zr}_{0.5}\text{O}_2$ films as well.

The XPS spectra were recorded on an SPECS spectrometer equipped with a PHOIBOS-150-MCD-9 hemispherical analyzer and a FOCUS-500 x-ray monochromator (Al $\text{K}\alpha$ radiation, 1486.74 eV, 200 W). An analysis of the integral intensities of XPS lines, carried out with taking into account

the atomic sensitivities of the elements, has shown that a film with $[\text{Hf}]/[\text{Zr}] = 1.05$ was obtained. A convolution of Gaussian and Lorentzian functions was used, for fitting the $\text{Hf}4f$, $\text{Zr}3d$ and $\text{O}1s$ peaks. The ion etching of the sample was performed using an ion gun (SPECS, model IQE 11/35), for oxygen vacancies generation. The Ar^+ ion energy, current density and beam angle were 1.25 keV, $8\text{--}10 \mu\text{A cm}^{-2}$, and 45° , respectively. Independently from the etching duration (5 and 30 min), the oxygen vacancies concentration was the same.

The first-principle modeling was made within the DFT and periodically arranged supercells model using the Quantum-ESPRESSO package [16]. The hybrid B3LYP exchange-correlation functional was used. The valence electron wavefunctions were decomposed in a plane wave basis with cutoff energy 65 Ry, with the core being considered through norm-conserving pseudopotentials. A 12-atom $\text{f-Hf}_{0.5}\text{Zr}_{0.5}\text{O}_2$ unit cell was obtained by the replacement of half of the Hf atoms with Zr atoms in the f-HfO_2 cell [17] followed by a subsequent relaxation of the structure. The choice of the atoms for the replacement was made from the principle of the cell total energy minimum. The structure includes four non-equivalent oxygen atoms: two four-coordinated Hf–Hf–Zr–Zr atoms (the corresponding O vacancy designated in what follows as $\text{V}_{\text{O}(\text{HHZZ})}$), different in the Hf–O and Zr–O bonds lengths, and two three-coordinated O atoms: Hf–Hf–Zr (oxygen vacancy denoted as $\text{V}_{\text{O}(\text{HHZ})}$) and Hf–Zr–Zr (oxygen vacancy designated as $\text{V}_{\text{O}(\text{HZZ})}$). The $\text{O}(\text{HHZZ})$ vacancies possess identical electronic structures; that is why, here, we present the calculation data for one of them. The oxygen vacancies are formed by the removal of oxygen from a 96-atom supercell obtained by a $2 \times 2 \times 2$ translation of the unit cell with a subsequent relaxation of all atoms.

The optimization of several O vacancies spatial arrangement in the supercell is realized according to the principle of the minimum formation energy, which was calculated as:

$$E_{\text{form}} = E_{\text{def}} - E_{\text{perf}} + N\mu_{\text{O}}$$

Here E_{perf} and E_{def} are the total energies of the perfect supercell, and supercell with the N oxygen vacancy, respectively, μ_{O} is the oxygen atom chemical potential, taken equal to half of the total oxygen molecule energy in the triplet state. All possible options for the second vacancy position were tested for a fixed single vacancy a , and its formation energies were compared to find the energy-favorable position. Similarly, the energy-favorable position of the third oxygen vacancy in the supercell was defined, but for a pair of fixed vacancies.

The five charge states of the oxygen vacancy in $\text{f-Hf}_{0.5}\text{Zr}_{0.5}\text{O}_2$ ($q = -2, -1, 0, 1, 2$) were considered. Because of using the periodic boundary conditions, the neutralizing uniform charge background method was employed in the calculations of charged oxygen vacancies. The supercell size separates the periodic defect images by about 10 \AA , and that provides the Coulomb interaction between the charged defects lower than 0.1 eV [18]. XPS were calculated

by summing the partial densities of filled states with weight factors equal to the corresponding photoionization cross-section values [19] and by smoothing using a Gauss function with $\sigma = 0.7 \text{ eV}$.

3. Results and discussion

Apart from the peaks due to Hf, Zr and O, the XPS analysis has revealed the presence of C in the sample (figure 2(a)). In the initial films, the atomic ratio $[\text{C}]/[\text{Zr}+\text{Hf}]$ was equal to 0.95 and, after the Ar^+ ion etching, this ratio was found to decrease to 0.4. This indicates the carbon localization on the film surface.

A low-intensity peak is observed at 531.9 eV (figure 2(b)), in the $\text{O}1s$ photoelectron spectrum. This peak can be identified as the one due to hydroxyl groups. The concentration of those groups also notably decreases after the samples ions etching. The binding energies of $\text{O}1s$ electrons for HfO_2 and ZrO_2 have close values in the range of 530.1–530.4 eV; that is why, in the XPS spectrum of $\text{Hf}_{0.5}\text{Zr}_{0.5}\text{O}_2$, these energies refer to one peak. Since photoelectrons, as they traverse the dielectric layer, spend part of their kinetic energy for plasmon excitation and interband electronic transitions, then the spectrum of the $\text{O}1s$ line reflects the photoelectron-energy losses spectrum (figure 2(c)), thus, enabling the estimate of the $\text{f-Hf}_{0.5}\text{Zr}_{0.5}\text{O}_2$ plasmon energy and bandgap energy E_g [20]. The onset of the band-to-band transitions excitation, which corresponds to E_g , can be identified using a linear interpolation of the $\text{f-Hf}_{0.5}\text{Zr}_{0.5}\text{O}_2$ absorption edge to the background level. For the examined samples, this procedure yields a value of $5.3 \pm 0.2 \text{ eV}$. This value is consistent with the energy 5.37 eV deduced from the $\text{f-Hf}_{0.5}\text{Zr}_{0.5}\text{O}_2$ transmission spectra [21] and with the data of [22], showing that the HfZrO_4 bandgap energy is $\sim 0.4 \text{ eV}$ smaller than those of HfO_2 and ZrO_2 , both energies being equal to 5.6–5.8 eV [23, 24]. The $\text{f-Hf}_{0.5}\text{Zr}_{0.5}\text{O}_2$ bandgap energy as calculated within the DFT in the present study is 5.7 eV. The overestimate, in comparison with the experimental value, can be attributed to the use of the B3LYP exchange-correlation functional which yields $E_g = 6.1 \text{ eV}$ for HfO_2 [25].

The broad peak with its maximum at an energy of $21.8 \pm 0.3 \text{ eV}$ higher than that of the $\text{O}1s$ line is due to the bulk plasmon excitation of valence electrons. This conclusion is confirmed by a simple estimate of plasmon energy $\hbar\omega_p$ for the free electron model; this energy is evaluated taking into account the $\text{O}2p^4$, $\text{Hf}6s^25d^1$ and $\text{Zr}5s^24d^1$ valence electrons and, also, the unit-cell volume of 141.2 \AA^3 , proved to be 21.6 eV.

The $\text{Hf}4f$ and $\text{Zr}3d$ photoelectron spectra of the initial sample surface can be fairly well approximated with single doublets (figures 2(d) and (e)). The energy position of the maximum of $\text{Hf}4f_{7/2}$, 17.05 eV corresponds to the Hf^{4+} state and coincides with the energy position of the same maximum in HfO_2 , which, according to literature data, falls in the range of 16.8–17.1 eV [26–28]. Similarly, the maximum of $\text{Zr}3d_{5/2}$ (182.3 eV) corresponds to the Zr^{4+} state and coincides with

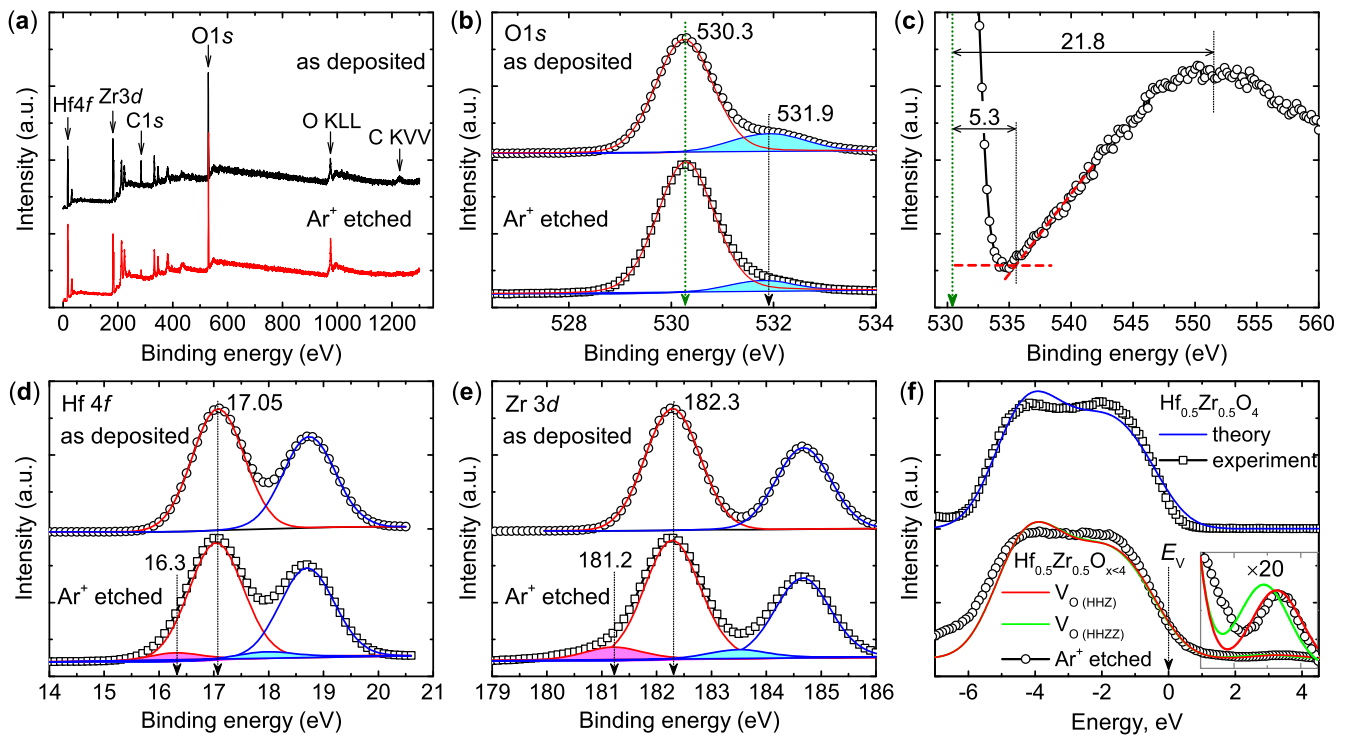


Figure 2. (a) XPS survey spectra of initial of the $f\text{-Hf}_{0.5}\text{Zr}_{0.5}\text{O}_2$ and after Ar^+ etching of the $f\text{-Hf}_{0.5}\text{Zr}_{0.5}\text{O}_2$. (b) $\text{O}1s$ photoelectron spectra of initial and after ion etching of the $f\text{-Hf}_{0.5}\text{Zr}_{0.5}\text{O}_2$ (symbols) and their deconvolution (lines). (c) $\text{O}1s$ photoelectron energy loss spectra. (d) $\text{Hf}4f$ photoelectron spectra of initial $f\text{-Hf}_{0.5}\text{Zr}_{0.5}\text{O}_2$ and that after ion etching (symbols) and their deconvolution (lines). (e) The same data for $\text{Zr}3d$ core level. (f) Valence band XPS of the initial $f\text{-Hf}_{0.5}\text{Zr}_{0.5}\text{O}_2$ and that after ion etching (symbols), in comparison with the calculated ones for the perfect crystal and for crystal with differently coordinated O vacancies (lines). The zero energy is taken as the valence band top.

the previously reported data for ZrO_2 , 181.9–182.3 eV [29–31]. After the Ar^+ ions etching, the $\text{Hf}4f$ and $\text{Zr}3d$ peaks broaden, and that provides an indication for some partial disorder of the near-surface region in the etched films (occurrence of defects, vacancies, etc). The $\text{Hf}4f$ and $\text{Zr}3d$ lines deconvolution into separate components allows revealing the peaks at energies 16.3 eV and 181.2 eV, respectively. Those peaks, are characteristic for Hf and Zr in non-stoichiometric oxides, where the metal atoms have smaller oxidation degrees (1+, 2+, and 3+) [7, 32]. After the ion etching, the proportion between the atomic concentrations of elements, $[\text{O}]/[\text{Zr}+\text{Hf}]$, becomes equal to 1.9. This value was obtained with taking into account the normalization of the corresponding data for the as deposited sample to the stoichiometric oxide. It can, therefore, be concluded that the $f\text{-Hf}_{0.5}\text{Zr}_{0.5}\text{O}_2$ ion etching leads to the film near-surface region depletion with oxygen.

The latter conclusion is confirmed by the comparison of experimental valence band XPS with the calculated XPS for the ideal $f\text{-Hf}_{0.5}\text{Zr}_{0.5}\text{O}_2$ crystal and for a crystal with oxygen vacancies (figure 2(f)). The calculated spectra are consistent with the experimental ones in terms of the spectral lines width and number of the main involved peaks. This result proves the adequacy of the used theoretical model. An asymmetric structure of the peaks in the calculated valence band XPS spectrum was previously observed for HfO_2 [13], and it was explained by the simplicity of the used theoretical XPS model. The $f\text{-Hf}_{0.5}\text{Zr}_{0.5}\text{O}_2$ ion etching broadens the XPS spectrum and induces a peak in the range of energies above

the valence band top. The calculated XPS spectra of $f\text{-Hf}_{0.5}\text{Zr}_{0.5}\text{O}_2$ with oxygen vacancies exhibit a peak at the same energy in the bandgap of the material. The energy position of the maximum of the calculated peak for the three-coordinated vacancy 3.4 eV above the valence band top coincides with the energy position of the experimental peak. The latter coincidence unambiguously proves the fact that the $f\text{-Hf}_{0.5}\text{Zr}_{0.5}\text{O}_2$ ion etching has resulted in the formation of an oxygen-deficient near-surface layer in the material.

The calculated bandgap peak intensity varies at the proportion to O vacancies concentration, and the experimental peak well coincides with the theoretical peak obtained by the calculation of one vacancy in the 96-atom supercell of $f\text{-Hf}_{0.5}\text{Zr}_{0.5}\text{O}_2$. Hence, the estimated O vacancies concentration in the examined ion etched film was $8.7 \times 10^{20} \text{ cm}^{-3}$. The calculated value of the atomic ratio $[\text{O}]/[\text{Zr}+\text{Hf}] \approx 1.97$ exceeds the value deduced from the XPS of the $\text{Hf}4f$, $\text{Zr}3d$ and $\text{O}1s$ levels. The theoretical value seems to be more trustworthy since the accuracy in determining the stoichiometry from the XPS data typically amounts to about 10%.

The formation of the XPS peak at an energy above the valence band top after the Ar^+ etching was previously observed in amorphous HfO_2 and ZrO_2 films [12, 13]. In both cases, along with a peak at 3 eV above the valence band top due to oxygen vacancies, the second equally intense peak at 1 eV was observed in the XPS spectrum. In the case of $f\text{-Hf}_{0.5}\text{Zr}_{0.5}\text{O}_2$, the second peak cannot be identified. Yet, the fact that the valence top edge in the etched film becomes gentler sloping does not exclude the possibility that such

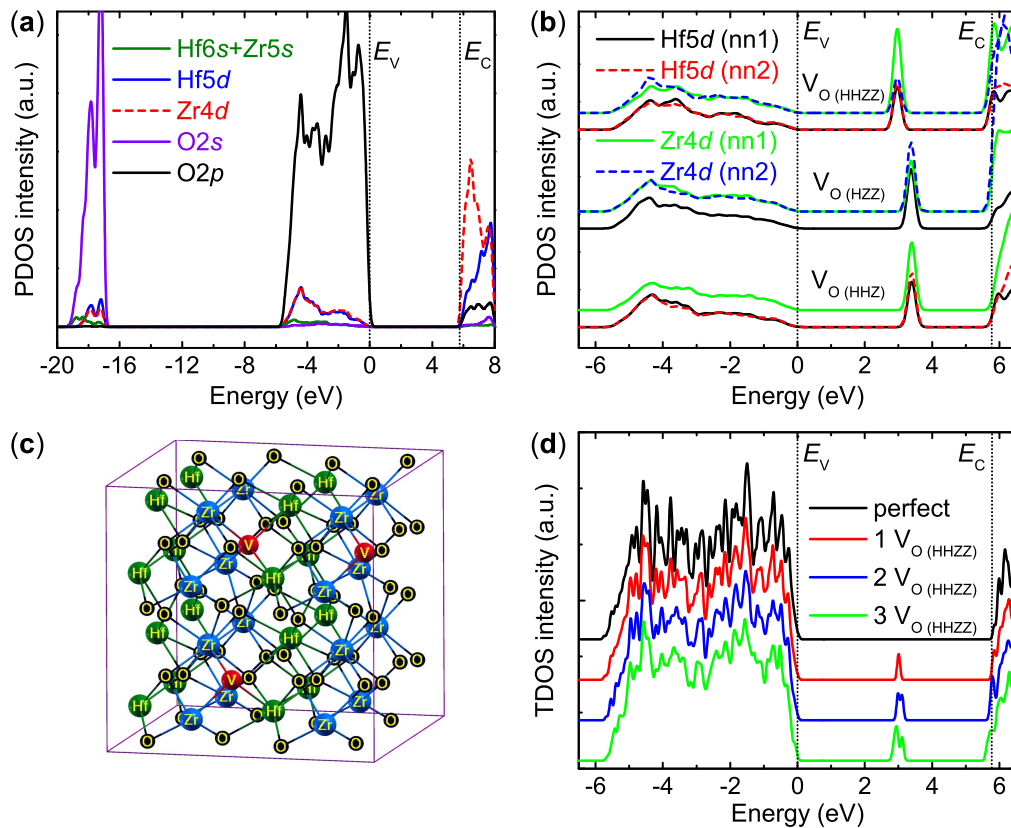


Figure 3. (a) PDOS spectra of perfect $f\text{-Hf}_{0.5}\text{Zr}_{0.5}\text{O}_2$; (b) PDOS spectra for the d electrons of the Hf and Zr atoms nearest to the O vacancy in different coordinations; (c) the perfect 96-atom supercell with the oxygen positions for vacancies creation marked in red; (d) TDOS spectra of the $f\text{-Hf}_{0.5}\text{Zr}_{0.5}\text{O}_2$ supercell having one, two and three O vacancies.

low-intensity peak is present in the XPS spectrum as well. In contrast to $f\text{-Hf}_{0.5}\text{Zr}_{0.5}\text{O}_2$, which XPS spectrum exhibits a low-intensity 3.4 eV peak, both for HfO_2 and ZrO_2 the ions etching with similar parameters produces a much more intense bandgap peak at a roughly same energy.

The total density of states (TDOS) and partial density of states (PDOS) spectra of $f\text{-Hf}_{0.5}\text{Zr}_{0.5}\text{O}_2$ show that the valence band in this material is primarily formed by O $2p$ states, and the conduction band—by Hf $5d$ and Zr $4d$ states (figure 3(a)). The Zr $4d$ state makes a greater contribution to the PDOS in the vicinity of the conduction band bottom E_C . The three-coordinated O vacancies introduce an occupied defect state at an energy of about 3.3 eV into the bandgap, and four-coordinated vacancies—an occupied defect state at the energy of 2.93 eV (figure 3(b)). For the monoclinic phase (m-) of ZrO_2 , similar calculations yield the defect level positions in the bandgap of 3.1 and 2.7 eV, respectively [33]. Also, the presence of oxygen vacancies leads to the formation of the states in the immediate vicinity of the conduction band bottom. A similar feature was earlier observed in m- HfO_2 [34].

The defect states are primarily formed by the $5d$ and $4d$ electrons of the Hf and Zr atoms nearest to the vacancy, respectively (figure 3(b)). For three-coordinated vacancies, the nearest neighboring (nn) atoms make roughly identical contributions to the defect level formation. In the case of the O(HHZZ) vacancy, one Zr atom induces a PDOS defect peak twice more intensive than the peaks induced by other atoms.

The latter points to the predominant charge density localization on one Zr atom and is confirmed by a small variation (decrease) of the effective charge value as calculated from the Löwdin occupation analysis. A defect-structure relaxation analysis has shown that this atom gets displaced toward the center of the vacancy at the distance of 0.04 Å, whereas the Hf atoms undergo the displacements as small as 0.01 Å; the second Zr atom, which initially was the most remote from the vacancy, gets displaced from the vacancy at the distance of 0.04 Å.

It can be hypothesized that it is oxygen polyvacancies (i.e. complexes of closely spaced oxygen vacancies) that are responsible for the appearance of the XPS peak above the valence band edge, because the formation of such defects during ion etching is quite probable. However, it was established that the removal of the second and third oxygen atoms from the $f\text{-Hf}_{0.5}\text{Zr}_{0.5}\text{O}_2$ supercell is energy-favorable from the four-coordinated HHZZ position, the vacancies being located at a large distance (≥ 6 nm) from each other. The $f\text{-Hf}_{0.5}\text{Zr}_{0.5}\text{O}_2$ 96-atom supercell with highlighted three oxygen atoms, the removal of which consumes less energy, is illustrated in figure 3(c). Two oxygen vacancies introduce two occupied states into the bandgap, three oxygen vacancies introduce three such states figure 3(d). The levels energy position almost coincides with the level position due to a single vacancy in the supercell. The latter points to a weak interaction between the vacancies. So, the vacancies can be

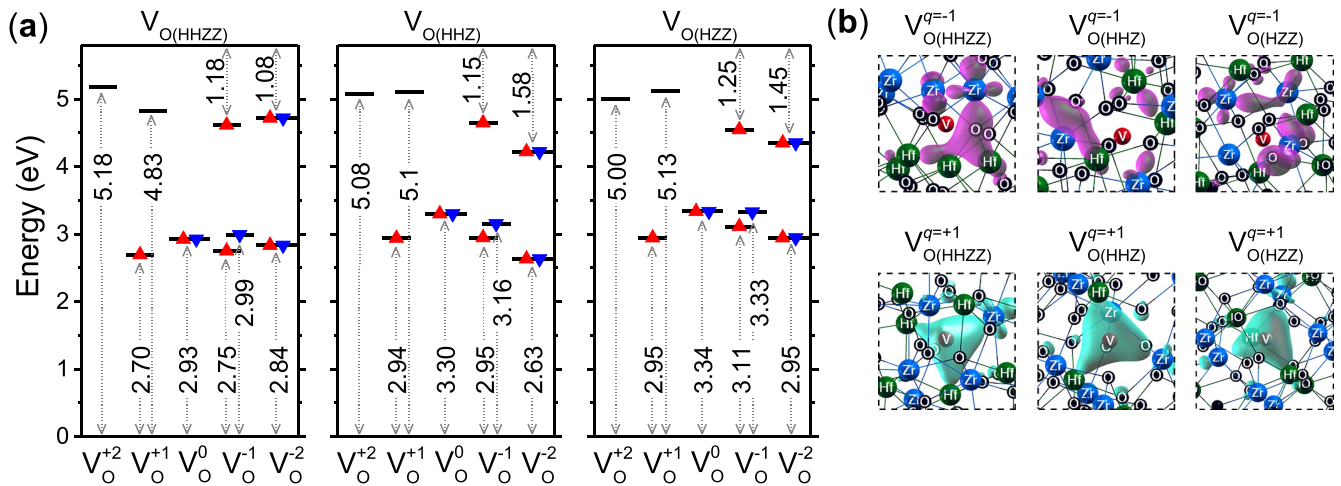


Figure 4. (a) The defect energy levels position in the f-Hf_{0.5}Zr_{0.5}O₂ bandgap caused by O vacancies in different coordinations in five charge states. Zero energy corresponds to E_V . (b) Isocharge density surfaces for the f-Hf_{0.5}Zr_{0.5}O₂ supercell with single negatively and positive charged O vacancies in different coordinations.

treated as independent defects. The vacancies independence is also supported by the formation energy values for the second and third oxygen vacancies in the supercell; these values being coincident with the formation energy of the first vacancy in the cell. Hence, the formation of oxygen polyvacancies in f-Hf_{0.5}Zr_{0.5}O₂ is energy-unfavorable. Interesting, on the contrary, a gain in the energy due to the oxygen vacancies clusterization process in the cubic, tetragonal and monoclinic phases of ZrO₂ with not more than two oxygen vacancies being in the vicinity of one Zr atom was established in [33]. Probably, due to this fact, f-Hf_{0.5}Zr_{0.5}O₂ film etching with Ar⁺ ions will result just in a weak enrichment of the surface region with the metal, in comparison with ZrO₂ [12] and HfO₂ [13] films.

Different charged states of V_O(HHZZ), V_O(HHZZ) and V_O(HHZZ) in f-Hf_{0.5}Zr_{0.5}O₂ form filled and empty defect states in the bandgap (figure 4(a)). The calculations give the levels located either in the midgap region or about 1.2 eV from the conduction band edge, the latter states being occupied for a negatively charged vacancy. The similar picture for charged oxygen vacancies was previously obtained for m-HfO₂ [34, 35] and m-ZrO₂ [8, 33].

The strongest localization of the extra electron is observed for the O(HZZ) vacancy. In this case, the vacancy levels positioned at 1.25 eV below E_C coincide with the thermal trap energy in amorphous and f-Hf_{0.5}Zr_{0.5}O₂ [13] films, as well as for HfO₂ [5], and close to 1.15 eV for ZrO₂ [36], obtained by comparing the experimental and theoretical current–voltage characteristics. The second added electron leads to the singlet defect state. The defect level from the neutral O vacancy, coinciding with the E_C , becomes deep for negatively charged O vacancies due to the strong atomic relaxation (a strong polaronic effect). The nn metal atoms are shifted toward the center of the vacancy an order of magnitude stronger than in the case of neutral O vacancy. It indicates a strong polaronic effect. In the +1 charged O vacancy, the remaining electron is localized near the middle of the f-Hf_{0.5}Zr_{0.5}O₂ bandgap, and second empty level appears at

1 eV below E_C . The fully ionized oxygen vacancy gives an empty state in the bandgap and about 1 eV below E_C .

The charged O vacancies defect peaks width lower than 0.1 eV in the TDOS spectra, as well as their depth, indicate the charge localization in space. The spin-polarized charge density spatial distribution of the positive and negative charge in the f-Hf_{0.5}Zr_{0.5}O₂ supercell also confirms the charge localization (figure 4(b)). Both negative and positive charges are localized in the O vacancy region and its first coordination sphere. The electron density of the O vacancy in state $q = +1$ is distributed evenly between the nearest metal atoms and it can be described as a bonding combination of the atomic orbitals of all nn Hf and Zr. The strong localization with its maximum in the O vacancy center and the behavior of the atomic relaxation have their typical structure of an F center. An additional localized electron is much weaker, and it leads to a charge density distribution preferentially among two metal atoms closest to each other.

Therefore, the DFT simulation of different charged states of oxygen vacancies in f-Hf_{0.5}Zr_{0.5}O₂ indicate that any type of oxygen vacancies in f-Hf_{0.5}Zr_{0.5}O₂ can act as electron and hole traps, in this way, participate in the charge transport.

4. Conclusion

In the present study, the atomic and electronic structure of oxygen vacancies in the orthorhombic noncentrosymmetric phase of f-Hf_{0.5}Zr_{0.5}O₂ was investigated. For the examined ALD film of f-Hf_{0.5}Zr_{0.5}O₂, the bandgap energy and the bulk plasmon energy were evaluated, which proved to be 5.3 ± 0.2 eV and 21.8 ± 0.3 eV, respectively. It is shown that the Ar⁺ ion etching of f-Hf_{0.5}Zr_{0.5}O₂ introduces additional lines in the region of smaller binding energies in the XPS spectrum of Hf4f and Zr3d levels and, also, it introduces a peak above the valence band top. The quantum-chemical calculations of the electronic structure of perfect and oxygen-deficient f-Hf_{0.5}Zr_{0.5}O₂ crystal provide a clear indication that

the peak observed in the XPS spectrum above the valence band edge is due to oxygen vacancies. The comparison between the calculated and experimental XPS spectra of the valence band provides a method for evaluating the oxygen vacancies concentration in the film near-surface region. The oxygen vacancies concentration in Ar^+ -etched $\text{f-Hf}_{0.5}\text{Zr}_{0.5}\text{O}_2$ amounts to $8.7 \times 10^{20} \text{ cm}^{-3}$. The energy positions of defect levels in the bandgap of $\text{f-Hf}_{0.5}\text{Zr}_{0.5}\text{O}_2$, due to oxygen vacancies in different charge states with different atomic coordinations, were identified. It was found that, although the formation of a four-coordinated oxygen vacancy is most energy-favorable, the experimental XPS peak observed at the energies above the valence band edge can be fairly well described by the peak calculated for the three-coordinated vacancy. The formation of non-interacting oxygen vacancies distant from each other proved to be more energy-favorable than that of oxygen polyvacancies. One can assume that Ar^+ etching can lead to forming Hf/Zr vacancies. However, according to our *ab initio* simulations, such kind of defects are not stable in several crystal modifications of $\text{Hf}_{0.5}\text{Zr}_{0.5}\text{O}_2$. Both electron and holes can localize in the oxygen vacancy, and the hole localization is much stronger. The electron localization on the oxygen vacancy in $\text{f-Hf}_{0.5}\text{Zr}_{0.5}\text{O}_2$ is caused by the polaronic effect. The calculated defect levels position for the negatively charged oxygen vacancy in $\text{f-Hf}_{0.5}\text{Zr}_{0.5}\text{O}_2$ is consistent with the previously defined experimental thermal trap ionization energy value. Thus, it was proved that the oxygen vacancy in $\text{f-Hf}_{0.5}\text{Zr}_{0.5}\text{O}_2$ is an amphoteric defect, i.e. it can act as both an electron trap and hole trap and participate in charge transport. As far as the oxygen vacancy acts as a charge trapping center in ferroelectric $\text{Hf}_{0.5}\text{Zr}_{0.5}\text{O}_2$ films, the defects will be pinning centers of ferroelectric domains and will lead to FRAM retention degradation [12]. Also, the traps create additional channel of the leakage currents, which is the cause of increased heat generation and energy consumption in $\text{Hf}_{0.5}\text{Zr}_{0.5}\text{O}_2$ -based electronic devices. In this case it is important for FRAM and FET industry to develop a synthesis technique $\text{Hf}_{0.5}\text{Zr}_{0.5}\text{O}_2$ that can provide oxygen-vacancy-less $\text{Hf}_{0.5}\text{Zr}_{0.5}\text{O}_2$ films. This issue is beyond the scope of this paper and require further research.

Acknowledgments

This work was supported by the Russian Science Foundation (Grant No. 14-19-00192). The simulation study was carried out using the Siberian Supercomputer Center (ICMMG SB RAS) resources. The authors thank Dr A M Markeev and Dr A G Chernikova for their $\text{f-Hf}_{0.5}\text{Zr}_{0.5}\text{O}_2$ film synthesis.

ORCID iDs

T V Perevalov  <https://orcid.org/0000-0003-0895-6202>
 D R Islamov  <https://orcid.org/0000-0002-5188-7049>
 V A Gritsenko  <https://orcid.org/0000-0003-1646-0848>
 I P Prosvirin  <https://orcid.org/0000-0002-0351-5128>

References

- [1] Muller J, Boscke T S, Schroder U, Mueller S, Brauhaus D, Bottger U, Frey L and Mikolajick T 2012 Ferroelectricity in simple binary ZrO_2 and HfO_2 *Nano Lett.* **12** 4318–23
- [2] Pustovarov V A, Perevalov T V, Gritsenko V A, Smirnova T P and Yelisseyev A P 2011 Oxygen vacancy in Al_2O_3 photoluminescence study and first-principle simulation *Thin Solid Films* **519** 6319–22
- [3] Robertson J and Wallace R M 2015 High- K materials and metal gates for CMOS applications *Mater. Sci. Eng. R* **88** 1–41
- [4] Afanas'ev V V, Stesmans A, Mrstik B J and Zhao C 2002 Impact of annealing-induced compaction on electronic properties of atomic-layer-deposited Al_2O_3 *Appl. Phys. Lett.* **81** 1678–80
- [5] Takeuchi H, Ha D and King T-J 2004 Observation of bulk HfO_2 defects by spectroscopic ellipsometry *J. Vac. Sci. Technol. A* **22** 1337–41
- [6] Kimura H, Mizuki J, Kamiyama S and Suzuki H 1995 Extended x-ray absorption fine-structure analysis of the difference in local structure of tantalum oxide capacitor films produced by various annealing methods *Appl. Phys. Lett.* **66** 2209–11
- [7] Gritsenko V A, Perevalov T V and Islamov D R 2016 Electronic properties of hafnium oxide: a contribution from defects and traps *Phys. Rep.* **613** 1–20
- [8] Hur J H, Park S and Chung U I 2012 First principles study of oxygen vacancy states in monoclinic ZrO_2 : interpretation of conduction characteristics *J. Appl. Phys.* **112** 113719
- [9] Islamov D R, Perevalov T V, Gritsenko V A, Cheng C H and Chin A 2015 Charge transport in amorphous $\text{Hf}_{0.5}\text{Zr}_{0.5}\text{O}_2$ *Appl. Phys. Lett.* **106** 102906
- [10] Islamov D R, Chernikova A G, Kozodaev M G, Markeev A M, Perevalov T V, Gritsenko V A and Orlov O M 2015 Charge transport mechanism in thin films of amorphous and ferroelectric $\text{Hf}_{0.5}\text{Zr}_{0.5}\text{O}_2$ *JETP Lett.* **102** 544–7
- [11] Pesic M et al 2016 Physical mechanisms behind the field-cycling behavior of HfO_2 -based ferroelectric capacitors *Adv. Funct. Mater.* **26** 4601–12
- [12] Morant C, Fernandez A, Gonzalezlopez A R, Soriano L, Stampfl A, Bradshaw A M and Sanz J M 1995 Electronic structure of stoichiometric and Ar^+ -bombarded ZrO_2 determined by resonant photoemission *Phys. Rev. B* **52** 11711–20
- [13] Perevalov T V, Aliev V S, Gritsenko V A, Saraev A A and Kaichev V V 2013 Electronic structure of oxygen vacancies in hafnium oxide *Microelectron. Eng.* **109** 21–3
- [14] Islamov D R, Chernikova A G, Kozodaev M G, Perevalov T V, Gritsenko V A, Orlov O M and Markeev A M 2017 Leakage currents mechanism in thin films of ferroelectric $\text{Hf}_{0.5}\text{Zr}_{0.5}\text{O}_2$ *ECS Trans.* **75** 123–9
- [15] Islamov D R, Chernikova A G, Kozodaev M G, Markeev A M, Perevalov T V, Gritsenko V A and Orlov O M 2017 Leakage currents mechanism in thin films of ferroelectric $\text{Hf}_{0.5}\text{Zr}_{0.5}\text{O}_2$ *J. Phys.: Conf. Ser.* **864** 012002
- [16] Giannozzi P et al 2009 QUANTUM ESPRESSO: a modular and open-source software project for quantum simulations of materials *J. Phys.: Condens. Matter* **21** 395502
- [17] Zeng Q F et al 2014 Evolutionary search for new high- k dielectric materials: methodology and applications to hafnia-based oxides *Acta Crystallogr. C* **70** 76–84
- [18] Foster A S, Lopez Gejo F, Shluger A L and Nieminen R M 2002 Vacancy and interstitial defects in hafnia *Phys. Rev. B* **65** 174117
- [19] Scofield J H 1976 Hartree-slater subshell photoionization cross-sections at 1254 and 1487 eV *J. Electron Spectrosc. Relat. Phenom.* **8** 129–37

- [20] Miyazaki S 2002 Characterization of high- k gate dielectric/silicon interfaces *Appl. Surf. Sci.* **190** 66–74
- [21] Ambriz-Vargas F, Kolhatkar G, Thomas R, Nouar R, Sarkissian A, Gomez-Yanez C, Gauthier M A and Ruediger A 2017 Tunneling electroresistance effect in a Pt/Hf_{0.5}Zr_{0.5}O₂/Pt structure *Appl. Phys. Lett.* **110** 093106
- [22] Hegde R I, Triyoso D H, Samavedam S B and White B E 2007 Hafnium zirconate gate dielectric for advanced gate stack applications *J. Appl. Phys.* **101** 074113
- [23] Kirm M, Aarik J, Jurgens M and Sildos I 2005 Thin films of HfO₂ and ZrO₂ as potential scintillators *Nucl. Instrum. Methods A* **537** 251–5
- [24] Afanas'ev V V, Stesmans A, Zhao C, Caymax M, Heeg T, Schubert J, Schubert J, Jia Y, Schlom D G and Lucovsky G 2004 Band alignment between (100)Si and complex rare earth/transition metal oxides *Appl. Phys. Lett.* **85** 5917–9
- [25] Gavartin J L, Muñoz Ramo D, Shluger A L, Bersuker G and Lee B H 2006 Negative oxygen vacancies in HfO₂ as charge traps in high- k stacks *Appl. Phys. Lett.* **89** 082908
- [26] Renault O, Samour D, Damlencourt J F, Blin D, Martin F, Marthon S, Barrett N T and Besson P 2002 HfO₂/SiO₂ interface chemistry studied by synchrotron radiation x-ray photoelectron spectroscopy *Appl. Phys. Lett.* **81** 3627–9
- [27] Fang Q *et al* 2004 Interface of ultrathin HfO₂ films deposited by UV-photo-CVD *Thin Solid Films* **453** 203–7
- [28] Jiang R, Xie E Q and Wang Z F 2006 Interfacial chemical structure of HfO₂/Si film fabricated by sputtering *Appl. Phys. Lett.* **89** 142907
- [29] Jeon T S, White J M and Kwong D L 2001 Thermal stability of ultrathin ZrO₂ films prepared by chemical vapor deposition on Si(100) *Appl. Phys. Lett.* **78** 368–70
- [30] Kim M S, Ko Y D, Hong J H, Jeong M C, Myoung J M and Yun I 2004 Characteristics and processing effects of ZrO₂ thin films grown by metal-organic molecular beam epitaxy *Appl. Surf. Sci.* **227** 387–98
- [31] Tsunekawa S, Asami K, Ito S, Yashima M and Sugimoto T 2005 XPS study of the phase transition in pure zirconium oxide nanocrystallites *Appl. Surf. Sci.* **252** 1651–6
- [32] Bespalov I, Datler M, Buhr S, Drachsel W, Rupprechter G and Suchorski Y 2015 Initial stages of oxide formation on the Zr surface at low oxygen pressure: an *in situ* FIM and XPS study *Ultramicroscopy* **159** 147–51
- [33] Perevalov T V and Islamov D R 2017 Atomic and electronic structure of oxygen polyvacancies in ZrO₂ *Microelectron. Eng.* **178** 275–8
- [34] Broqvist P and Pasquarello A 2006 Oxygen vacancy in monoclinic HfO₂: a consistent interpretation of trap assisted conduction, direct electron injection, and optical absorption experiments *Appl. Phys. Lett.* **89** 262904
- [35] Chen T J and Kuo C L 2011 First principles study of the structural, electronic, and dielectric properties of amorphous HfO₂ *J. Appl. Phys.* **110** 064105
- [36] Jegert G, Kersch A, Weinreich W, Schroder U and Lugli P 2010 Modeling of leakage currents in high-kappa dielectrics: three-dimensional approach via kinetic Monte Carlo *Appl. Phys. Lett.* **96** 062113